ACS APPLIED MATERIALS & INTERFACES

Research Article

www.acsami.org

Performance of Doxorubicin-Conjugated Gold Nanoparticles: Regulation of Drug Location

Teng Cui,[†,‡,⊥] Juan-Juan Liang,[†,‡,⊥] Huan Chen,[§] Dong-Dong Geng,[†,‡] Lei Jiao,[‡] Jian-Yong Yang,[‡] Hai Qian,[‡] Can Zhang,*[,‡] and Ya Ding*[,†]

[†]State Key Laboratory of Natural Medicines, Department of Pharmaceutical Analysis, [‡]Jiangsu Key Laboratory of Drug Discovery for Metabolic Diseases, Center of Drug Discovery, and [§]Department of Biochemistry, School of Life Science and Technology, China Pharmaceutical University, Nanjing 210009, China

Supporting Information

ABSTRACT: Drug-conjugated gold nanoparticles (GNPs), which are generally constructed with many molecules of thiol-terminated polyethylene glycol (PEG)-drug decorated on their surfaces via a thiol-Au covalent bond, are promising and efficient nanoprodrugs. However, because of the exposure of the hydrophobic drug molecules on the surface of the conjugate, *in vivo* stability, opsonization, and subsequent inefficient therapy become the main issues of this system. To solve these problems without complicating the structures of gold conjugates, herein we propose a method to change the relative position of PEG and the drug. A novel gold conjugate (GNP-NHN═Dox-mPEG) with doxorubicin (Dox) shielded by PEGylation on the surface of GNPs is designed. It demonstrates improved solubility, stability, and dispersion and achieves a two-step stimulus-responsive drug release in response to an acidic environment in lysosomes and then esterase in the cytoplasm. This unique manner of release enables the cytoplasm to act as a reservoir for sustained drug delivery into the nucleus to improve antitumor efficacy *in vivo*. The intratumoral drug concentrations of the conjugate reach 14.4 ± 1.4 μg/g at 8 h, a two-fold increase in the drug concentration compared with that of the doxorubicin hydrochloride group. This molecular design and regulation approach is facile but important in modulating the *in vivo* performance of nanovehicles and demonstrates its vital potential in developing effective nanoparticle-based drug delivery agents.

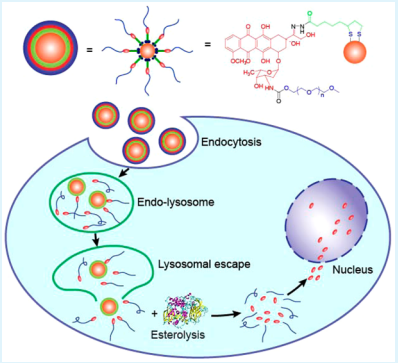

KEYWORDS: *Doxorubicin-conjugated gold nanoparticles, drug location, two-step drug release, lysosomal escape, treatment efficacy improvement*

1. INTRODUCTION

Drug-conjugated gold nanoparticles (GNPs) have become increasingly popular for applications in both gene and chemical drug delivery.[1,2] Incorporating drugs on the surfaces of GNPs enhances the biological specificity and therapeutic efficacy of the drugs without causing serious systemic toxicity.[3,4] So far, GNPs have been conjugated with a variety of therapeutics including ciprofloxacin,[5] paclitaxel (PTX),[6,7] doxorubicin (Dox),[8,9] curcumin,[10] and chloroquine[11] to achieve their desired therapeutic effects. Current research studies have been mainly focused on the fabrication of multifunctional conjugates,[12,13] endocytosis-enhanced cellular uptake,[14] and the relevant applications for overcoming multidrug resistance.[9,15,16] Although it is crucial to control the properties and functions of gold conjugates by regulating their basic structure, very few studies regarding these concerns have been reported.

As a special cross-linked nanoprodrug with a "hard" core, an ideal drug-conjugated GNP system is expected to be stable and inactive in circulation, selectively target diseased tissues, and convert to an active structure through a normal metabolic process.[17,18] To realize this stability and selectivity, oligo- and polyethylene glycols (PEG) have generally been employed as spacers to covalently connect GNPs and drug molecules at their termini.[6−8,19] By adjusting the molecular weights (MWs) of PEGs and the sensitivities of chemical bonds to environmental stimuli at the target site, the physicochemical and pharmaceutical properties of drug-conjugated GNPs can be finely controlled both *in vitro* and *in vivo*.[7,9,15,16,20] However, because of the presence of the hydrophobic drug on the conjugate surface, a hydrophobic shell is formed, which decreases the system's solubility and dispersion. In addition, drug molecules in the outermost layer are easily absorbed by various proteins in the physiological environment, which subsequently leads to opsonization. These processes may reduce the plasma concentration and circulation time of therapeutics as well as the drug release in tumor tissues. Therefore, solving the problems of the conjugates described above is a worthwhile challenge.

In this work, a novel lipoic acid (LA)-modified PEG derivative of Dox (LA-NHN═Dox-mPEG) with a PEG MW

Received: December 27, 2016
Accepted: February 20, 2017
Published: February 20, 2017

DOI: 10.1021/acsami.6b16669
ACS Appl. Mater. Interfaces 2017, 9, 8569−8580

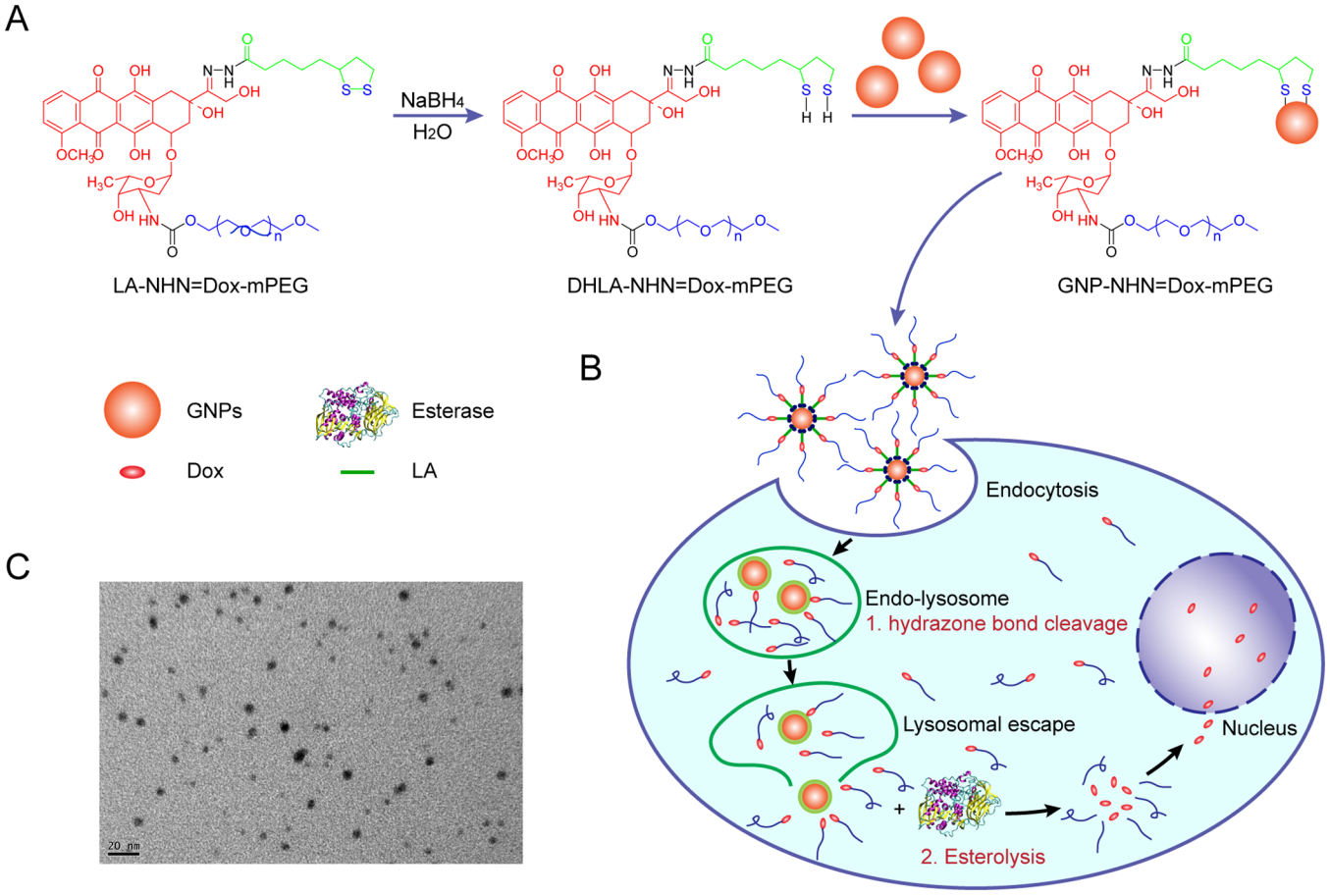

Figure 1. (A) The structure of GNP-NHN═Dox-mPEG and (B) an illustration of its intracellular drug release mechanism. (C) TEM image of GNP-NHN═Dox-mPEG. The scale bar is 20 nm.

of 1000 Da was designed, followed by the fabrication of GNP-NHN═Dox-mPEG, as shown in Figure 1A. Instead of using PEG as the spacer, Dox is bimodified by LA and mPEG on the carbonyl and amino groups, respectively. Through a ring-opening reaction in the presence of sodium borohydride, LA-NHN═Dox-mPEG is reduced into its dihydrolipoate (DHLA-NHN═Dox-mPEG), and then GNP-NHN═Dox-mPEG with a hydrophilic mPEG outer layer is prepared. It is worth noting that this method to change the relative position of PEG and the drug is the easiest way to solve the solubility, dispersion, and stability issues mentioned above without complicating the gold conjugate structure. In addition, for selective drug release in tumor cells, a hydrazone bond and a carbamate bond were introduced in LA-NHN═Dox-mPEG to achieve a two-step stimulus-responsive drug release. The release process includes the liberation of Dox-mPEG in acidic lysosomes and then free Dox in cytoplasm catalyzed by esterase (Figure 1B). From this unique release manner, the cytoplasm acts as a reservoir for continuous drug release in tumor cells, and the gold conjugates demonstrate improved liver tumor treatment efficacy compared to that of doxorubicin hydrochloride (Dox·HCl) after i.v. administration. The molecular design and modulation of the gold conjugates offer new perspectives on the performance improvement of nanocarriers by controlling their basic structures.

2. MATERIALS AND METHODS

2.1. Chemicals and Instruments. Tetrachloroauric acid ($HAuCl_4$), dicyclohexylcarbodiimide (DCC), 4-dimethylaminopyridine (DMAP), trifluoroacetic acid (TFA), hydrazine hydrate ($NH_2NH_2{\cdot}H_2O$), and 4-nitrophenyl chloroformate (NPC) were purchased from Sinopharm Chemical Reagent Co., Ltd. (Shanghai, China). Polyethylene glycol monomethyl ether (mPEG) with an average molecular weight of 1000 Da was purchased from Sigma-Aldrich (USA). Dox·HCl was obtained from HuaFeng United Technology Co., Ltd. (Beijing, China). High performance liquid chromatography (HPLC) spectral-grade reagents were used as the mobile phase during HPLC analysis. Other reagents were analytical grade and used as received. Distilled and deionized water (>18 MΩ, Purelab Classic Corp., USA) was used in all the experiments.

The morphology and distribution of the gold conjugates were imaged with a JEM-200CX TEM (JEOL, Japan) with a 200 kV acceleration voltage. The hydrodynamic diameter and zeta potential of the conjugates were measured with a Zetasizer 3000HS instrument (Malvern Instruments, Malvern, UK) using 633 nm He−Ne lasers at 25 °C. Ultraviolet−visible (UV−vis) spectra were detected with a UV3600 spectrophotometer (Shimadzu, Japan). The emission spectra were measured using a Shimadzu RF-5301 fluorescence spectrometer. The chemical structures of all the organic intermediates and products were determined with a Nicolet 6700 FT-IR spectrometer (Thermo Scientific, USA). The ^1H and ^{13}C NMR spectra were recorded on a Bruker (AVANCE) AV-400 spectrometer. Thermogravimetric analysis (TGA) was carried out with a thermal gravimetric analyzer (TG 209 F1, Netzsch, Germany). The gold concentration was measured by Optima 5300DV ICP-MS (PE, USA). The concentrations of Dox and Dox-mPEG were determined using a Shimadzu-20AT series analytical reverse-phase high-performance liquid chromatograph (RP-HPLC)

DOI: 10.1021/acsami.6b16669
ACS Appl. Mater. Interfaces 2017, 9, 8569−8580

with a fluorescence detector (λ_{ex} = 480 nm, λ_{em} = 560 nm). A C18 column (4.6 × 250 mm^2, Thermo Scientific, USA) was used to separate the analytes at 1 mL/min and 30 °C. A mobile phase of 10 mM aqueous ammonium acetate/acetonitrile (60:40, v/v) containing 0.1% formic acid was used. All HPLC runs were performed in triplicate.

2.2. Preparation of GNP-NHN═Dox-mPEG. Citrate-protected GNPs with an average size of approximately 3.4 ± 0.6 nm were prepared following previous reports.[3,4,20] The synthesis procedure of LA-NHN═Dox-mPEG is shown in Supporting Information, Figure S1. Structural characterizations of the starting materials, intermediates, and final products of LA-NHN═Dox-mPEG using Fourier transform infrared spectroscopy (FT-IR) and ^{1}H and ^{13}C nuclear magnetic resonance spectroscopy (NMR) are presented in Supporting Information (Figure S3−S11).

For the Dox modification on the GNP surfaces, LA-NHN═Dox-mPEG (0.52 mmol) was dissolved in 2 mL of methanol and cooled in an ice bath. To the solution of LA-NHN═Dox-mPEG, a cold solution of $NaBH_4$ (29.5 mg, 0.78 mmol) was added. The solution was stirred for 1 h at 0 °C to form the dihydrolipoic acid (DHLA)-modified PEG derivative of Dox (DHLA-NHN═Dox-mPEG). The S−Au bond was formed after addition of the above citrate-stabilized GNPs (10 mL). The reaction solution was dialyzed against deionized water for 72 h (MWCO = 7000 kDa) and lyophilized to a dark red powder of GNP-NHN═Dox-mPEG.

2.3. *In Vitro* Drug Release. For the investigation of *in vitro* drug release, Dox-mPEG was synthesized as shown in Supporting Information, Figure S2. Structural characterizations of the intermediates and final products of Dox-mPEG using FT-IR and ^{1}H/^{13}C NMR are also presented in the Supporting Information.

The release of Dox and Dox-mPEG was carried out using dialysis.[20−22] Accurately weighed amounts of dried GNP-NHN═Dox-mPEG (14.8 mg containing 4.0 mg Dox) were dispersed in 3 mL of phosphate-buffered saline (PBS, 0.03 M) at pH 7.4 and divided into three 1 mL solutions. The solutions were placed in dialysis bags with a molecular weight cutoff of 7000 Da. To investigate the drug release behavior, the dialysis bags were placed in the release medium (PBS containing Tween 80, 0.1%, v/v) at different pH values (5.5, 6.5, and 7.4). Further Dox release from Dox-mPEG was carried out in the presence of esterase from porcine liver (lyophilized powder, ≥ 15 units/mg solid, Sigma-Aldrich, USA). Dox-mPEG (11.6 mg containing 4.0 mg Dox) was dissolved in 3 mL of 0.03 M PBS at pH 7.4 and divided into three 1 mL solutions. Each solution was diluted into 10 mL of PBS (0.03 M and pH 7.4) containing 20 units of esterase.[23] The release solutions were stirred at 150 rpm and 37 °C. At predetermined time intervals, 200 μL aliquots of the release medium were withdrawn for RP-HPLC analysis and replaced with fresh medium. All assays were performed in triplicate.

2.4. Cell Culture. Human hepatocellular liver carcinoma cell line (HepG2) was purchased from the China Center for Type Culture Collection (Shanghai, China). For cell tests, cells were seeded in cell culture plates using Dulbecco's modified Eagle's medium (DMEM) with 10% fetal bovine serum (FBS) and incubated at 37 °C under a humidified atmosphere with 5% CO_2 for 24 h to reach 80% confluence.

2.5. Cellular Uptake. *2.5.1. Cellular Uptake Mechanism Studies.* HepG2 cells were seeded in cell culture dishes for 24 h to reach a confluence of 80%. The media were removed, and cells were washed with PBS twice. After successive incubation with cell culture media containing chlorpromazine (10 μg/mL), genistein (200 μg/mL), and wortmannin (100 ng/mL) for 1 h each, cells were further incubated with GNP-NHN═Dox-mPEG at a Dox dose of 5 μg/mL for another 3 h. The excess medium was removed, and cells were washed with PBS, trypsinized, and centrifuged. The intracellular gold concentration was detected by ICP-MS. The results were represented as the mean ± SD (n = 3).

2.5.2. Cellular Uptake of the Gold Conjugate. The experimental procedure was the same as in the cellular uptake mechanism studies except that no inhibitors were added, and the incubation periods with GNP-NHN═Dox-mPEG were 4 and 12 h.

2.5.3. Intracellular Distribution of the Gold Conjugate. HepG2 cells were seeded in six-well plates and incubated for 24 h to reach 80% confluence. Citrate-protected GNPs and GNP-NHN═Dox-mPEG were diluted using cell culture medium to a gold concentration of 2.0 μg/mL and added to cell culture plates. After incubation for 4 and 12 h, respectively, excess medium was removed, and the cells were washed with cold PBS, trypsinized, centrifuged, and imaged under an 80 kV JEM-1011 transmission electron microscope. The pretreatment method of the TEM samples was discussed in the previous report.[20]

2.6. Cytotoxicity. For the cytotoxicity assay, HepG2 cells were seeded in a 96-well plate (1.2 × 10^4 cells/well) and incubated in a growth medium with 5% FBS containing Dox·HCl, LA-NHN═Dox-mPEG, GNP-NHN═Dox-mPEG, or Dox-mPEG at different Dox concentrations for 24 h. After two washes with 200 μL of PBS, the cell inhibition rates were detected using a Cell Counting Kit-8 (CCK-8, Sigma-Aldrich, USA) by comparing the absorbance at 450 nm with control wells containing only the cell culture medium. The data are presented as the means ± SD (n = 5), with each experiment repeated three times.

2.7. Intracellular Tracking and Drug Release. The cells were seeded in confocal dishes at a density of 1 × 10^5 cells/mL and grown for 24 h to reach a confluence of 60%. Cell culture medium with 5% FBS containing GNP-NHN═Dox-mPEG with a dose of 5 μg/mL Dox was added. After incubations of 4, 12, 24, and 48 h, cells were washed with PBS thrice. Before observation by confocal microscope (Ti−C2, Nikon) at 1000× magnification, the lysosome was stained with LysoTracker Green DNA-26 (500 nM) at 37 °C for 30 min, and the nuclei were dyed using Hoechst 33342 (1 μg/mL) at 37 °C for 15 min.

2.8. Pharmacokinetic Studies. Healthy Sprague−Dawley rats (male, 200 ± 20 g) were used to examine the pharmacokinetics of GNP-NHN═Dox-mPEG using Dox·HCl as a reference. Rats were randomly divided into two groups (n = 5). Both Dox·HCl and GNP-NHN═Dox-mPEG were intravenously administered through the tail vein with an equivalent dose of 5 mg/kg of Dox. Blood samples (0.5 mL) were collected from the plexus venous at various times (0.08, 0.17, 0.25, 0.5, 1, 2, 4, 8, 12, 24, and 48 h) into heparinized tubes. The plasma samples were collected after immediate centrifugation at 12 000 rpm for 10 min and stored at −20 °C until analysis. A 0.1 mL aliquot of plasma was added to 10 μL of daunorubicin as the internal standard (IS), mixed with 0.2 mL of methanol to extract the Dox and IS, and subjected to plasma protein precipitation by vigorous vortexing. After centrifugation at 15 000 rpm for 3 min, the supernatant was concentrated under vacuum. The residue was dissolved in 0.2 mL of mobile phase and centrifuged at 15 000 rpm for 3 min, and the supernatant was analyzed by RP-HPLC as described above.

2.9. *In Vivo* Antitumor Efficacy. Healthy male ICR mice (20 ± 2 g) were purchased from the Comparative Medicine Centre of Yangzhou University (Certificate number: SCXK (Su) 2012−0004). Heps cells (Hepatoma solidity) were kindly provided by Nanjing University and were maintained as an ascites tumor in ICR mice. Heps cell suspensions containing 10^6 cells per 0.1 mL were implanted subcutaneously into the right axillary space. All the animals were pathogen free and were allowed free access to food and water. The experiments were carried out in compliance with the National Institute of Health Guide for the Care and Use of Laboratory Animals.

The tumor-bearing mice were subjected to antitumor activity studies after the tumor volume reached 200 mm^3. Animals with a tumor after Heps tumor inoculation were divided into three groups: saline, Dox·HCl, and GNP-NHN═Dox-mPEG. These formulations were diluted in saline. Tumor-bearing mice were injected through the tail vein with 5 mg/kg of Dox in the indicated formulation at 2-day intervals. Tumor volume was calculated by the following equation: tumor volume (mm^3) = (length × width^2)/2. At the end of the experiment, tumor tissues were excised, washed with saline, and weighed. The data were presented as the mean ± SD (n = 5). To evaluate the toxicity of the three formulations, the tumor-bearing mice in the survival rate experiment were also injected through the tail vein

DOI: 10.1021/acsami.6b16669
ACS Appl. Mater. Interfaces 2017, 9, 8569−8580

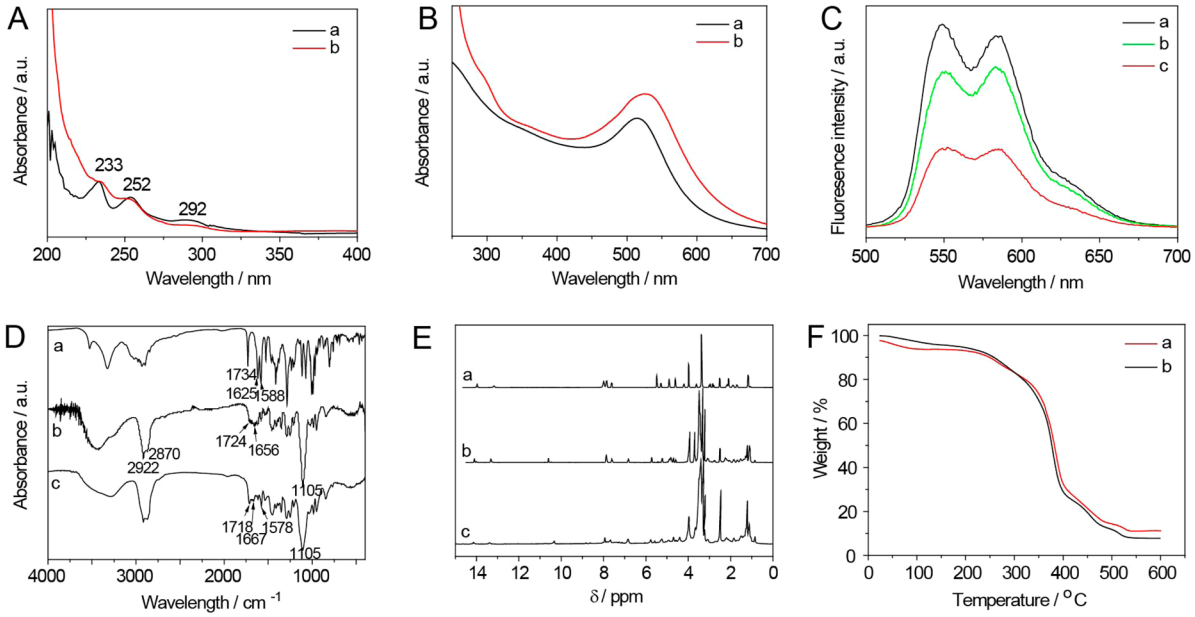

Figure 2. UV−vis spectra of (A) (a) Dox and (b) LA-NHN═Dox-mEPG and (B) (a) citrate-protected GNPs and (b) GNP-NHN═Dox-mEPG. (C) Fluorescence emission spectra, (D) FT-IR spectra, and (E) ^{1}H NMR spectra of (a) Dox·HCl, (b) LA-NHN═Dox-mPEG, and (c) GNP-NHN═Dox-mPEG. (F) TGA results of GNP-NHN═Dox-mPEG after (a) 12 h and (b) 72 h dialysis.

with 5 mg/kg of Dox in the indicated formulation at 2-day intervals for 30 days (n = 10).

2.10. Histological Analysis. The excised tumor tissues were fixed with 4% paraformaldehyde. The samples were processed and sectioned, and thin tissue sections were stained with hematoxylin and eosin (H&E) or TdT-mediated dUTP nick end labeling (TUNEL) using a TUNEL apoptosis detection kit (Roche, USA). The H&E- or TUNEL-stained sections were observed using Eclipse CI and Eclipse TI-SR microscopes (Nikon Optical Co., Ltd., Japan), respectively.

2.11. Biodistribution. ICR male mice (20 ± 2 g) with a tumor volume of 200 mm^3 after Heps tumor inoculation were randomly divided into two groups: (1) Dox·HCl and (2) GNP-NHN═Dox-mPEG. Each group was injected intravenously through the tail vein with the indicated formulation at a dose of 5 mg/kg Dox. After administration, mice were sacrificed at predetermined time points (0.5, 1, 4, 8, 12, 24, and 48 h, n = 5 at each time point), and heart, liver, spleen, lung, kidney, and tumor tissues were collected and stored at −20 °C until analysis. The collected tissues were homogenized with 800 μL of saline, and 100 μL of the homogenate was added to 10 μL of daunorubicin as the IS, mixed with 0.2 mL of methanol to extract the Dox and IS, and subjected to plasma protein precipitation by vigorous vortexing. After centrifugation at 15 000 rpm for 3 min, the supernatant was concentrated under vacuum. The residue was dissolved in 0.2 mL of mobile phase and centrifuged at 15 000 rpm for 3 min, and the supernatant was then analyzed by RP-HPLC as described above. The calibration curves of the tissues displayed good linearity.

2.12. Statistical Analysis. All the results are presented as the mean ± SD. The data were analyzed by one-way analysis of variance (ANOVA) with the appropriate Bonferroni correction to determine significant differences for multiple comparisons. P < 0.05 was considered to be statistically significant.

3. RESULTS AND DISCUSSION

3.1. Preparation and Characterization. The structure of GNP-NHN═Dox-mPEG is illustrated in Figure 1A, in which the Dox molecule is bifunctionalized and inserted between GNP and mPEG. The hydrophilic mPEG shell at the outermost layer of the conjugate causes the high solubility, dispersibility, and stability of GNP-NHN═Dox-mPEG. The solubility of GNP-NHN═Dox-mPEG in water is approximately 30 mg/mL Dox; this is equivalent to 25-times the solubility of Dox (1.18 mg/mL) and three-times the solubility of Dox·HCl (10 mg/mL). Even after lyophilization, GNP-NHN═Dox-mPEG exhibits desirable solubility. A clear solution and a monodisperse state for the GNP-NHN═Dox-mPEG sample can be observed for more than 2 weeks (Figure 1C). Changes of UV−vis absorption intensity at 520 nm as a function of time is shown in Supporting Information, Figure S12. Except for the sample in the acidic medium (0.03 M PBS at pH 5.5), the decay in the optical absorbance of the particle suspension was negligible for the GNP-NHN═Dox-mPEG conjugate (less than 7.5% in 10 h). This result indicates that the conjugate is stable in buffers with neutral pH values (pH 7.4; curve a), elevated salt concentrations (0.2 M PBS, pH 7.4; curve c), and in the presence of serum (curve d).

With the modification of DHLA-NHN═Dox-mPEG, the hydrodynamic diameter and zeta potential of the gold conjugate in water are 179.0 ± 7.5 nm and −0.95 ± 0.65 mV, respectively. The small size (less than 200 nm)[24] and nearly neutral surface charge of the conjugate are beneficial for escaping the reticuloendothelial system (RES) when applied in *in vivo* tumor therapy.

UV−vis spectra of Dox and its derivative (LA-NHN═Dox-mPEG) are shown in Figure 2A (curves a and b), which presents three characteristic peaks at 233, 252, and 292 nm arising from the aromatic ring structure of Dox. Citrate-protected GNPs display a characteristic UV−vis absorption spectrum, with a surface-localized plasmon resonance band at 515 nm (Figure 2B, curve a), which reflects the existence of GNPs with diameters of approximately 3−4 nm. With the modification of DHLA-NHN═Dox-mPEG, the UV−vis spectrum of GNP-NHN═Dox-mEPG demonstrated both organic and red-shifted inorganic absorbances at 292 and 525 nm (Figure 2B, curve b), respectively, which indicated the successful modification of DHLA-NHN═Dox-mPEG on the

DOI: 10.1021/acsami.6b16669
ACS Appl. Mater. Interfaces 2017, 9, 8569−8580

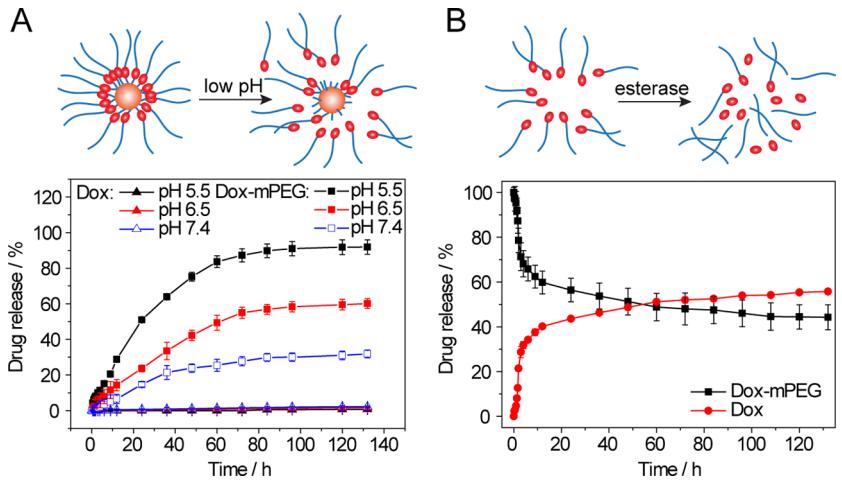

Figure 3. (A) *In vitro* Dox and Dox-mPEG release from GNP-NHN═Dox-mPEG in 0.03 M PBS at pH 5.5, 6.5, and 7.4. (B) Drug release plots of Dox-mPEG in the presence of porcine liver esterase (0.03 M PBS at pH 7.4). The amount of released drug was determined by RP-HPLC. Data points represent mean ± SD (n = 3).

surfaces of GNPs. Compared to Dox·HCl (Figure 2C, curve a), when Dox was chemically bifunctionalized, the fluorescence intensity of LA-NHN═Dox-mPEG decreased to 76.3% and 83.2% at 550 and 588 nm, respectively (Figure 2C, curve b). This fluorescence decrease is attributed to the redistribution of the electron cloud in Dox by the hypochromic effect.[25] After GNPs were conjugated with DHLA-NHN═Dox-mPEG, the fluorescence intensities at both 550 and 588 nm decreased even further (Figure 2C, curve c). This is based on the fluorescence resonance energy transfer (FRET) process between Dox and the GNPs.[26−28]

The organic shell structure of the gold conjugate was characterized using FT-IR and ^{1}H NMR. In comparison to Dox (Figure 2D, curve a), the FT-IR spectrum of LA-NHN═Dox-mPEG (Figure 2D, curve b) showed new peaks at 2922 and 2870 cm^{-1} that are assigned to $-CH_2$ groups in mPEG.[29] The absorption band at 1724 cm^{-1} is attributed to the newly formed ester bonds. The characteristic bands between 1600 and 1384 cm^{-1} are associated with the substituted benzene in Dox. The peaks for the C═N and N−H stretches at approximately 1420 and 3293 cm^{-1}, respectively, reveal the existence of hydrazone bonds. These results support the chemical structure of LA-NHN═Dox-mPEG shown in Figure 1A. The FT-IR spectrum of GNP-NHN═Dox-mPEG (Figure 2D, curve c) showed similar signals to those of LA-NHN═Dox-mPEG, except that some absorbances broadened, which indicated the successful modification of DHLA-NHN═Dox-mPEG on the gold surface.[29]

^{1}H NMR spectra for the test samples are shown in Figure 2E. In comparison with the proton NMR signals of Dox (curve a), the ^{1}H NMR spectrum of LA-NHN═Dox-mPEG (curve b) exhibited a new and broad resonance at 3.5 ppm corresponding to protons of mPEG connected to Dox via amide bonds, while also showing the characteristics peaks of Dox. The additional chemical shifts at about 2.3, 1.5, and 1.4 ppm revealed the existence of LA in the conjugate, and the broad signal over 10 ppm can be attributed to the proton of the hydrazone bond inserted between LA and Dox molecules. In addition to the signals of Dox, PEG, LA, and the hydrazone bond, the protons of the methyl group in the structure of mPEG appear at 3.2 ppm, which support the successful derivation of mPEG molecule on the distal end of LA-NHN═Dox-mPEG. In the spectrum of GNP-NHN═Dox-mPEG (curve c), broadened signals are also observed, which indicate the successful modification of DHLA-NHN═Dox-mPEG on the gold surface.[29]

To maximize the drug loading capacity (DLC) of the conjugate, excessive LA-NHN═Dox-mPEG was added in the prepared solution, and the unmodified compound was removed by the dialysis method. The TGA curves of GNP-NHN═Dox-mPEG are seen in Figure 2F after dialysis for 12 and 72 h. These two samples displayed similar organic and gold content (approximately 88.8% organic and 11.2% gold). The DLC of the conjugate is calculated to be 27.3% by calculating the individual molar mass of Dox and LA-NHN═Dox-mPEG as 543.52 g/mol and 1770 g/mol, respectively.[20] The minimum period of dialysis in the conjugate preparation was set at 12 h.

3.2. *In Vitro* Drug Release. *In vitro* drug release and mechanism studies of GNP-NHN═Dox-mPEG were performed, with results shown in Figure 3. On the basis of the bimodification structure of LA-NHN═Dox-mPEG (Figure 1A), free Dox is expected to be released under the synergistic conditions of the weak acid environments in tumor tissue or organelles and the high levels of esterase in the cytoplasm of tumor cells. Thus, a drug release experiment was conducted in medium containing esterase and in media at different pH values. For the conjugate, it is interesting that minute quantities of the drug were released in the presence of the esterase from porcine liver at pH 7.4 (data not shown here) and that the drug release is dependent on the solution pH value (Figure 3A). These results demonstrate the stability of the conjugate in circulation due to the protection effect of mPEG and the high density of the organic shell that reduces the adsorption and hydrolysis of the conjugate by esterase.[20] However, when the conjugate enters the tumor cell, pH has an important effect on the bond cleavage of hydrazone in GNP-NHN═Dox-mPEG.

The plots for the percentage of drug released from GNP-NHN═Dox-mPEG as a function of time at different pH values are shown in Figure 3A; its release behavior displays several features. First, the drug released from GNP-NHN═Dox-mPEG at different pH values is not in the form of Dox, but primarily in the form of Dox-mPEG. This result demonstrates the successful cleavage of the hydrazone bond between LA and Dox-mPEG. Second, the release rate and degree of the Dox-

DOI: 10.1021/acsami.6b16669
ACS Appl. Mater. Interfaces 2017, 9, 8569−8580

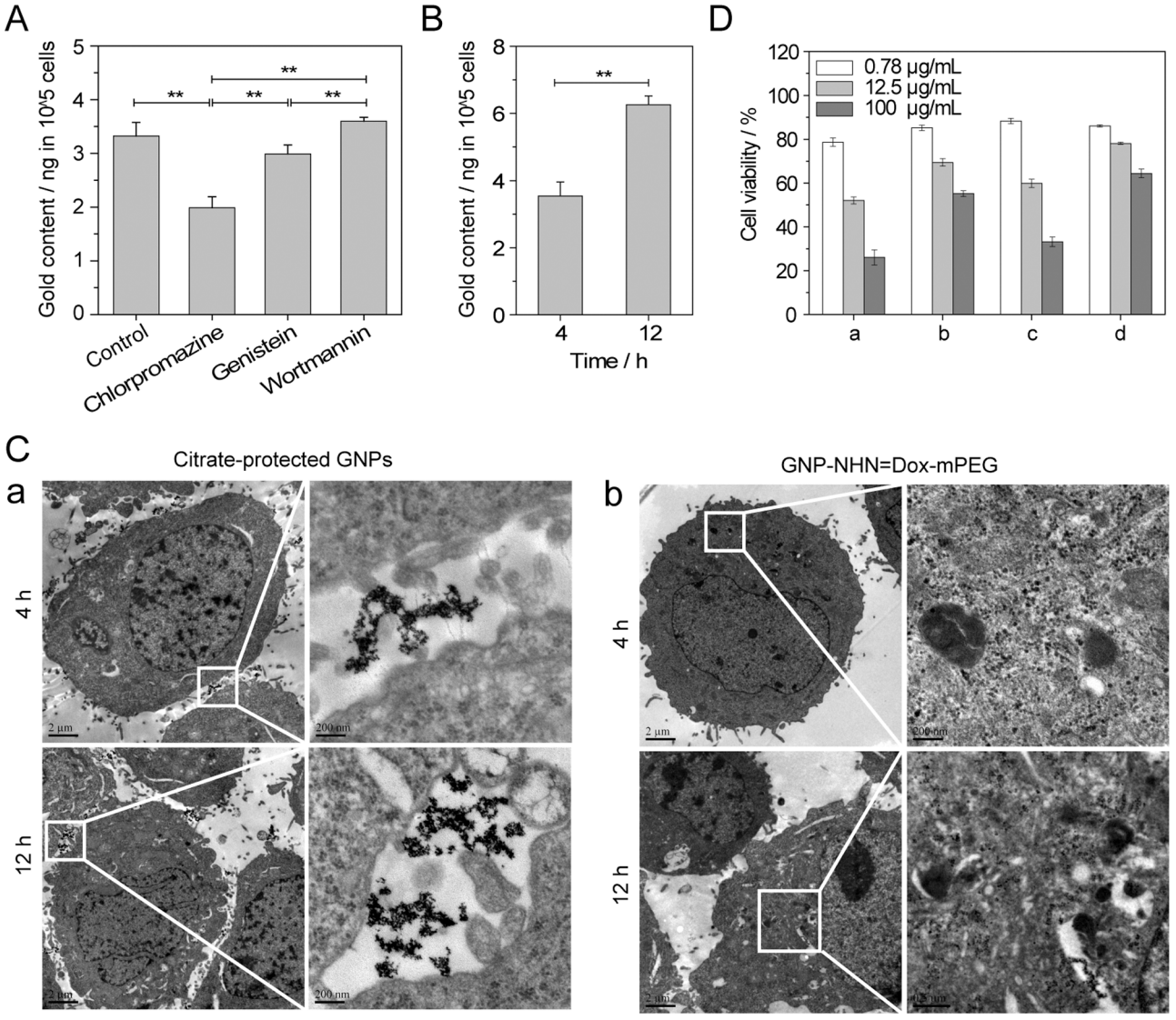

Figure 4. Gold contents inside HepG2 cells treated with GNP-NHN═Dox-mPEG (at a dose of 5 μg/mL Dox): (A) in the absence and presence of different inhibitors, chlorpromazine (10 μg/mL), genistein (200 μg/mL), or wortmannin (100 ng/mL) and (B) at different time points, 4 or 12 h. Data points were detected by ICP-MS assay and represent mean ± SD (n = 3). (C) TEM images of HepG2 cells after incubation with (a) citrate-protected GNPs and (b) GNP-NHN═Dox-mPEG for 4 or 12 h. (D) The cell viability of (a) Dox·HCl, (b) LA-NHN═Dox-mPEG, (c) GNP-NHN═Dox-mPEG, and (d) Dox-mPEG toward HepG2 cells for 24 h. Data points represent mean ± SD (n = 5).

mPEG segment are affected by pH value in the following order: pH 5.5 > pH 6.5 > pH 7.4. Only GNP-NHN═Dox-mPEG at pH 5.5 fully released its payload during the experimental period (132 h). At 132 h, only 31.9% of Dox-mPEG was released at pH 7.4, which is equal to one-third of the amount released at pH 5.5 (91.8%). This result indicates that GNP-NHN═Dox-mPEG will be stable *in vivo* before being taken up by tumor cells. When the conjugate enters acidic conditions such as the tumor microenvironment[30] and acidic organelles (e.g., lysosomes and endosomes),[31] the Dox-mPEG will be liberated. The released Dox-mPEG would further accumulate in tumor cells and act as a PEG prodrug until it is hydrolyzed by esterase in cytoplasm.

Although esterase is widely distributed in the human body, its overexpression in tumor cells has been reported and is an increasing focus in drug-sensitive delivery.[20,23,32] However, at low pH values (such as 5.5 and 6.5), the esterase became a white precipitate in the release medium and loses its activity. Thus, the dissociation of Dox from the Dox-mPEG segment in the presence of esterase at pH 7.4 was carried out separately (Figure 3B). The esterase-induced hydrolysis plots demonstrate that with increasing time, the Dox release increased followed by a decrease in the percentage of Dox-mPEG. The hydrolysis rate is rapid in the first 12 h and then slows to a plateau due to the lack of fresh esterase in the solution.

Therefore, the drug release behaviors described above showed effective Dox liberation via a two-step mechanism—the initial hydrazone bond breakage under acidic pH followed by the hydrolysis of the ester bond in the presence of esterase. This process is depicted in Figure 1B. To confirm our hypothesis inside tumor cells, we examined the cellular uptake mechanism, cytotoxicity, and intracellular tracking and drug release.

3.3. Cellular Uptake and Cytotoxicity. To reveal the cellular uptake mechanism of GNP-NHN═Dox-mPEG, chlorpromazine, genistein, and wortmannin were used to inhibit clathrin-mediated endocytosis, membrane cave-like depression-mediated endocytosis, and macropinocytosis,[33,34]

DOI: 10.1021/acsami.6b16669
ACS Appl. Mater. Interfaces 2017, 9, 8569−8580

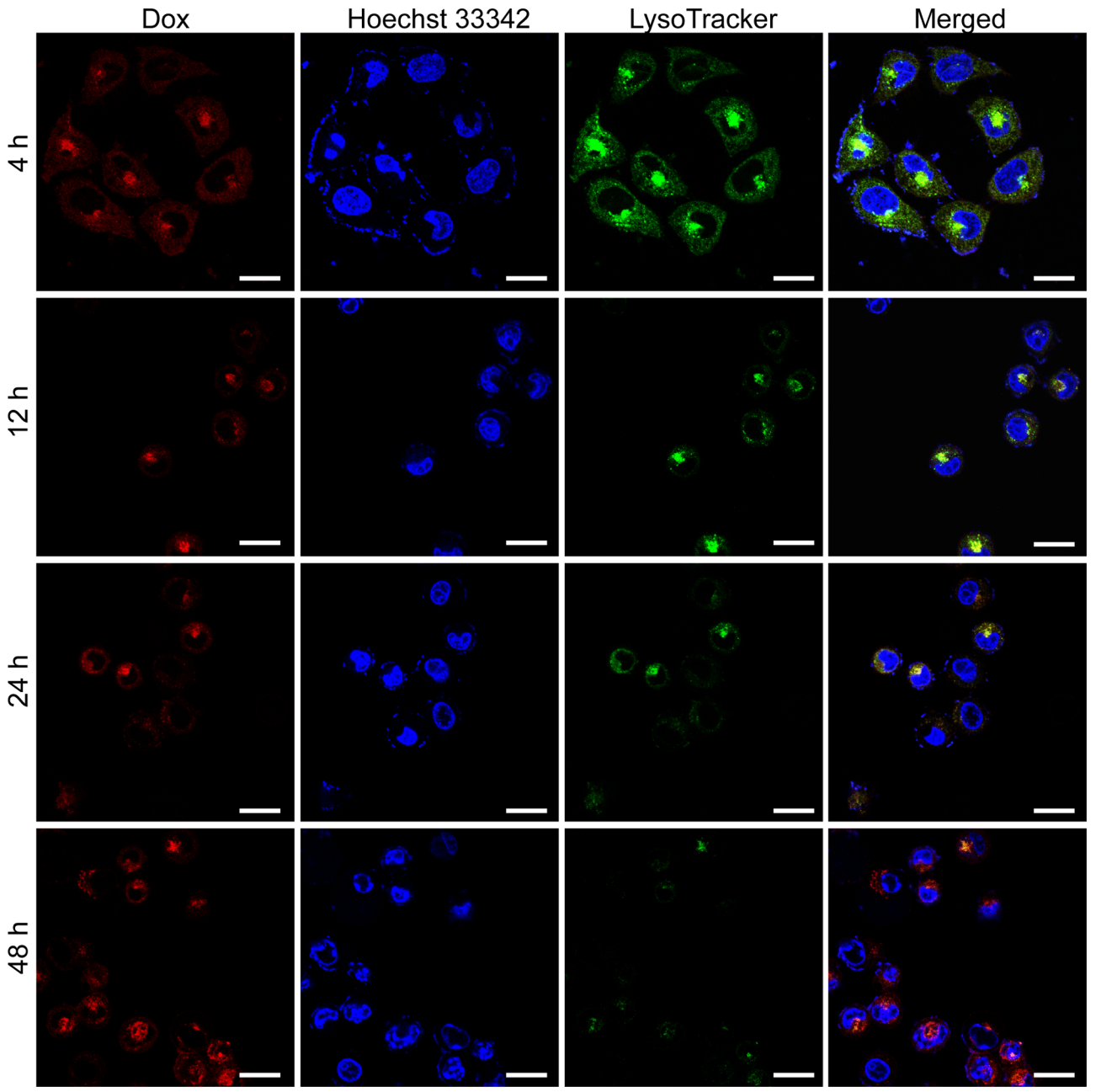

Figure 5. CLSM images of HepG2 cells for intracellular tracking of the conjugate at incubation times of 4, 12, 24, and 48 h with a dose of 5 μg/mL Dox. Scale bar is 20 μm.

respectively. The inhibitor was incubated with the cells for 1 h before the addition of GNP-NHN═Dox-mPEG. The intracellular gold content under the addition of these inhibitors was detected by ICP-MS and is shown in Figure 4A. The chlorpromazine displayed the strongest inhibition of cellular uptake, which indicated that clathrin-mediated endocytosis was the main uptake mechanism of GNP-NHN═Dox-mPEG.

Because of the endocytosis-induced cellular intake process[35] of the integrated conjugate and the high payload of DHLA-NHN═Dox-mPEG on the gold surface, the Dox concentration inside HepG2 cells could greatly increase. As shown in Figure 4B, the gold content inside HepG2 cells was 3.54 ± 0.41 ng and 6.26 ± 0.26 ng in every 10^5 cells at 4 and 12 h, respectively.

After incubation with GNP-NHN═Dox-mPEG (equivalent to 5 μg/mL Dox) for 4 and 12 h, the HepG2 cells were washed and observed by TEM (Figure 4C). Citrate-protected GNPs with the same gold content of the conjugate were used as the control. As shown in Figure 4C (image a), many citrate-protected GNPs remained outside and between the cells. Few particles were internalized by HepG2 cells due to their negatively charged surface protected by the citrate salt. In contrast, GNP-NHN═Dox-mPEG was present and remained in the cytoplasm of HepG2 cells after 4 and 12 h of incubation (Figure 4C, image b). This result indicated that, due to their surface modification, gold conjugates were unable to enter the nucleus via the nanosized gaps between nuclear pores (~9 nm)[36] even though the average size of the gold core is only approximately 3 nm. After 4 h incubation, the particles dispersed efficiently. No agglomerations were observed due to the repulsion interactions between mPEG molecules located

DOI: 10.1021/acsami.6b16669
ACS Appl. Mater. Interfaces 2017, 9, 8569−8580

A

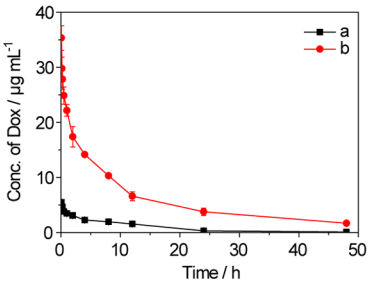

B

Pharmacokinetic parameters of the Dox·HCl solution and GNP-NHN=Dox-mPEG.

Parameter	Dox·HCl	GNP-NHN=Dox-mPEG
C_{max} (μg/mL)[a]	5.84 ± 0.41	38.39 ± 6.22**
$t_{1/2}$ (h)[b]	9.00 ± 0.22	18.78 ± 2.00**
$AUC_{0-\infty}$ (h·mg/L)[c]	42.40 ± 1.13	308.95 ± 14.26**
MRT (h)[d]	10.81 ± 0.39	23.13 ± 2.78**
CL (L/h/kg)[e]	0.12 ± 0.00	0.03 ± 0.00**
V_d (L/kg)[f]	1.53 ± 0.08	0.88 ± 0.08**

Date represent mean value ± SD, n=5.

*p<0.05, **p<0.01 versus Dox group (one-sample t-test).

[a] C_{max}, the maximum plasma concentration.

[b] $t_{1/2}$, plasma half life.

[c] $AUC_{0-\infty}$, area under the plasma concentration-time curve.

[d] MRT, mean residence time.

[e] CL, clearance rate.

[f] V_d, apparent volume of distribution.

Figure 6. (A) Plasma concentration−time profiles of Dox in rats following intravenous administration of (a) Dox·HCl and (b) GNP-NHN=Dox-mPEG at a Dox dose of 5 mg/kg. (B) Pharmacokinetic parameters of Dox·HCl and GNP-NHN=Dox-mPEG. Data represent the mean ± SD (n = 5).

on the particle surfaces. Images of GNP-NHN=Dox-mPEG group after 12 h incubation showed that some of the black particles were located in small vesicles inside the cytoplasm. This indicated the stagnation of some gold conjugates in organelles such as endosomes and lysosomes at 12 h. In such an acidic environment, Dox-mPEG segments are released, and particles appear to stick to each other to form a gold wire. The distribution of the gold cores inside cells confirmed that the conjugate would stay in the cytoplasm, thereby acting as a reservoir for the sustained release of free Dox.

As presented in Figure 4D, compared to LA-NHN=Dox-mPEG (column b) and its degradation product Dox-mPEG (column d), GNP-NHN=Dox-mPEG (column c) displayed higher cytotoxicity in HepG2 cells. This can be attributed to the enhanced cellular uptake of LA-NHN=Dox-mPEG with the help of GNPs and the subsequent release of free Dox molecules from the conjugate. However, the cytotoxicity of GNP-NHN=Dox-mPEG was slightly lower than the same Dox amount of Dox·HCl (column a) within 24 h. This can be explained by the sustained drug release behavior of GNP-NHN=Dox-mPEG inside cells, showing relatively slower cell killing activity than the Dox·HCl group, which has a rapid drug diffusion driven by the concentration gradient between the inner and outer cell membranes.

3.4. Intracellular Tracking and Drug Release. To investigate the intracellular tracking and drug release of the conjugate, confocal laser scanning microscopy (CLSM) was employed, and the imaging results are shown in Supporting Information, Figures S13 and Figure 5. In the case of Dox·HCl, the drug diffused in the cell quickly, including the cytoplasm and nucleus, after 4 h incubation due to the driving force from the concentration gradient (Supporting Information, Figure S13). In contrast, after 4 h incubation of GNP-NHN=Dox-mPEG, most of the red fluorescence of Dox and the green fluorescence of LysoTracher overlapped, which indicated the endocytosis and lysosomal localization of the conjugate (Figure 5). At 12 h, clear overlapping yellow fluorescence and shrinkage of HepG2 cells can also be seen in the GNP-NHN=Dox-mPEG group, which demonstrate the successful detachment of Dox-mPEG segments from the conjugate in acidic lysosomes and the subsequent cell killing ability generated by the released Dox from Dox-mPEG segments. In addition, after 12 h, the green fluorescence for the lysosome stain was very weak even though we used the same concentration of LysoTracher, and the intensity of the yellow fluorescence also decreased. This phenomenon implied the destruction of lysosomes and the successful lysosomal escape of the conjugate.

Since Dox must localize into the nucleus to perform its function[37] and the clathrin-mediated endocytosis and lysosomal escape of the conjugate have been confirmed as mentioned above, the nuclear distributions of the released Dox are important in this study. From Figure 5, we can find that the GNP-NHN=Dox-mPEG group always showed brighter red fluorescence intensity in the cytoplasm than in the nucleus, even after 48 h incubation. This confirmed a gradual liberation of free Dox from the Dox-mPEG segments that stayed in the cytoplasm and waited to be hydrolyzed by esterase. Thus, the cytoplasm here acted as a drug reservoir, which ensures a continuous Dox concentration inside the nucleus.

3.5. Pharmacokinetic Studies. After intravenous administration of Dox·HCl and GNP-NHN=Dox-mPEG in rats, the plasma drug concentration−time profiles were characterized using an RP-HPLC method with a fluorescence detector (λ_{ex} = 480 nm and λ_{em} = 560 nm). As shown in Figure 6A, the plasma Dox concentration after GNP-NHN=Dox-mPEG administration was much higher than that obtained in the Dox·HCl-treated group from 5 min to 48 h. It is worth noting that this higher plasma concentration of normalized Dox is in the form of Dox-mPEG rather than free Dox. This result is consistent with the *in vitro* drug release features shown in Figure 3A. The pharmacokinetic parameters of Dox in two formulations are presented in Figure 6B. For GNP-NHN=Dox-mPEG, the area under the plasma concentration−time curve ($AUC_{0-\infty}$) was 308.95 ± 14.26 h mg/L, which was approximately 7.29-times that of Dox·HCl (42.40 ± 1.13 h mg/L), and the corresponding total body clearance (CL) was 0.03 ± 0.00 L/h/kg, one-fourth that of Dox·HCl (0.12 ± 0.00 L/h/kg). For the combined mPEG-prodrug form in blood, these data suggest that the conjugate group displayed slower elimination of Dox, longer plasma half-life ($t_{1/2}$), and longer mean residence time (MRT) compared to Dox·HCl, which confirmed the longer circulation characteristics of GNP-NHN=Dox-mPEG *in vivo*.

3.6. *In Vivo* Antitumor Efficacy. Antitumor efficacy was evaluated in ICR mice bearing Heps tumors. The changes in

DOI: 10.1021/acsami.6b16669
ACS Appl. Mater. Interfaces 2017, 9, 8569−8580

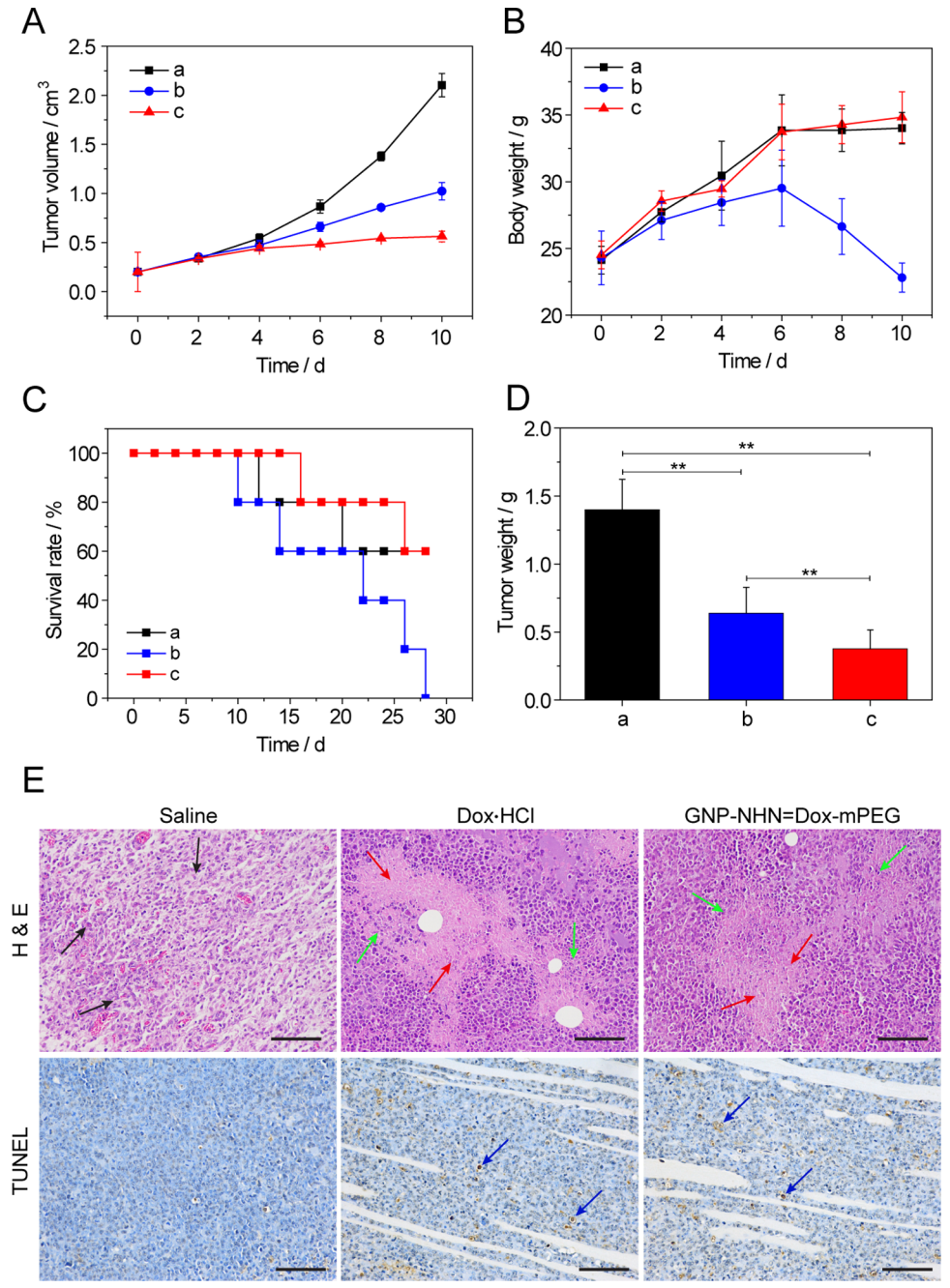

Figure 7. (A–D) *In vivo* antitumor efficacy of (a) saline, (b) Dox·HCl, and (c) GNP-NHN═Dox-mPEG in Heps tumor xenograft ICR mouse models. (A) tumor volume changes, (B) body weight changes, and (C) survival rates of the three groups of tumor-bearing mice during the 30-day treatment (n = 10), and (D) tumor tissue weight 10 days postinjection. Each point in panels A, B, and D represents the mean ± SD (n = 5). (E) Histological observation of tumor tissue sections (stained with H&E) and detection of apoptosis in tumor tissue sections (stained by TdT-mediated dUTP nick end labeling using a TUNEL kit, Roche, USA) from control and test groups 10 days postinjection. The scale bar is 100 μm.

tumor volume, body weight, survival rate, and final tumor weight of mice treated with saline, Dox·HCl, and GNP-NHN═Dox-mPEG are presented in Figure 7A–D. Tumor growth was significantly suppressed in the group treated with GNP-NHN═Dox-mPEG compared to those treated with saline and Dox·HCl (Figure 7A). Although the mice in the GNP-NHN═Dox-mPEG group had the smallest tumor size, their body weight (34.8 ± 1.9 g) was the heaviest, and the increment of their body weight (10.3 g) exceeded those of the other groups (Figure 7B, curve c). At the same time, the body weight of the saline group also increased quickly (Figure 7B, curve a), which is partly due to the rapid growth of tumor tissues as shown in Figure 7A (curve a). In contrast, the body weight of the Dox·HCl group increased at the beginning and decreased as the tumor volume increased, which indicated that the quality of life in Dox·HCl-treated mice was significantly decreased. The Dox·HCl group showed the highest body weight reduction (1.5 g, Figure 7B, curve b), which demonstrates the high toxicity of Dox·HCl *in vivo*. To further evaluate the toxicity of the test formulations, tumor-bearing mice in the survival rate experiments continued to receive intravenous injections in the indicated formulation at 2-day

DOI: 10.1021/acsami.6b16669
ACS Appl. Mater. Interfaces 2017, 9, 8569–8580

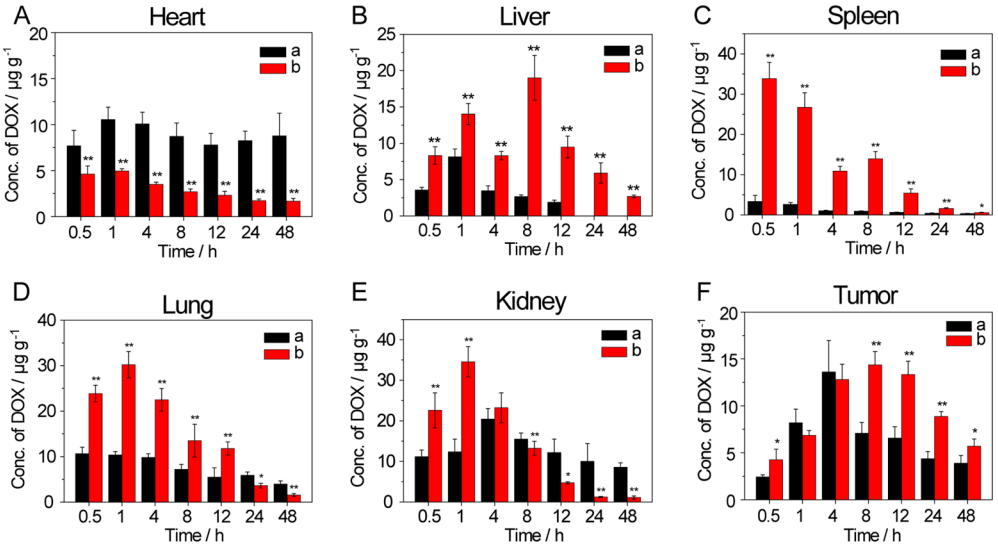

Figure 8. Biodistribution profiles of Dox concentrations in normal tissues including (A) heart, (B) liver, (C) spleen, (D) lung, (E) kidney, and (F) tumor tissues of tumor-bearing mice following intravenous injection of (a) Dox·HCl and (b) GNP-NHN═Dox-mPEG samples at a Dox dose of 5 mg/kg for different periods. Each point represents the mean ± SD (n = 5).

intervals. After the 28-day treatment, the mice in the Dox·HCl group were all dead, and the experiment was terminated (Figure 7C), while the survival rates of the saline and GNP-NHN═Dox-mPEG-treated groups after 28 days were 60%. These results demonstrated that the treatment with GNP-NHN═Dox-mPEG not only effectively prolongs life, but also shows reduced systemic toxicity *in vivo*.

To determine the extent of tumor damage in response to the conjugate, histological examination of H&E- and TUNEL-stained tumor tissue sections 10 days postinjection was performed (Figure 7E). There was no damage in the tumors in the saline-treated group, as a large number of tumor cells with irregularly shaped nuclei were observed (black arrow). However, significant necrosis was present in both Dox-containing groups (red arrow), and many inflammatory cells can be seen around the necrosis region (green arrow). Large necrosis regions were observed in tumors from the GNP-NHN═Dox-mPEG group, confirming the effective therapeutic efficacy of the gold conjugate. It was believed that the excellent therapeutic efficacy of the gold conjugate was due to its long circulation time and successful passive tumor targeting in tumor tissues. Histologic sections stained by TUNEL further revealed the apoptosis of tumor tissues after treatment with the test formulations. Many more brown dots presented in the tumor sections of mice treated by Dox·HCl and GNP-NHN═Dox-mPEG (blue arrow), which demonstrated significantly greater apoptosis of tumor cells than in the saline group. However, tumor tissue sections stained by H&E and TUNEL showed that there was no significant difference in tumor necrosis and apoptosis between these two Dox-treated groups. Therefore, biodistribution studies were performed to determine the tumor targeting and drug accumulation ability of the gold conjugate in comparison to Dox·HCl.

3.7. Biodistribution. Dox concentrations in the normal (including heart, liver, spleen, lung, and kidney) and tumor tissues of tumor-bearing mice treated with Dox·HCl and GNP-NHN═Dox-mPEG were detected and are shown in Figure 8. The data presented in the biodistribution results (Figure 8) are the normalized Dox concentrations calculated from the Dox-mPEG segments. It is known that cardiotoxicity is the main side effect of Dox,[38] and the concentration and retention of Dox in the heart is closely related with the toxicity of Dox-containing formulations. As shown in Figure 8A, Dox concentrations of the GNP-NHN═Dox-mPEG group in heart tissue were much lower than those of the Dox·HCl group at all time points after administration. This result suggests that, in association with Dox-mPEG formation, GNP-NHN═Dox-mPEG exhibited lower retention and more rapid elimination of Dox in the heart and thus exhibited less cardiotoxicity than Dox·HCl.

In tumor tissues, Dox concentrations in the Dox·HCl group increased in the first 4 h and then decreased rapidly. This result can be explained by the rapid drug distribution of free Dox in the whole body and subsequent quick elimination from the circulation, which is consistent with the pharmacokinetic results of Dox·HCl (Figure 6). In the case of GNP-NHN═Dox-mPEG, the normalized Dox concentrations exceeded those of the Dox·HCl group from 8−48 h after administration and reached a maximum at 8 h (Figure 8F). At this time, the peak value (14.36 ± 1.43 μg/g) was over twice that of the Dox·HCl group (7.08 ± 1.15 μg/g). This phenomenon was due to the protection effect of mPEG on the outer layer of the particle, which caused sustained circulation and effective passive tumor targeting via an enhanced permeability and retention effect *in vivo*.[39] In other normal tissues, including liver, spleen, lung, and kidney (Figure 8, B−E), the GNP-NHN═Dox-mPEG group appeared to show a higher early accumulation. However, the rapid elimination rate of the drug and its formation (Dox-mPEG) caused minor injury in normal tissues. Therefore, the enhanced accumulation and controlled drug release in tumor tissues ensured that higher amounts of Dox were delivered to tumor cells, which resulted in increased therapeutic efficacy and decreased side effects.

4. CONCLUSION

The results reported in this work show that using a simple method to change the relative PEG and drug positions can solve the main issues of drug-conjugated GNPs. For the as-prepared GNP-NHN═Dox-mPEG, the Dox is shielded by mPEGylation. The mPEG moiety observed as a protective shell on the outer layer of the conjugates ensured that the solubility,

DOI: 10.1021/acsami.6b16669
ACS Appl. Mater. Interfaces 2017, 9, 8569−8580

stability, dispersion, and biocompatibility of the Dox-conjugated GNPs improved significantly. The desirable size (179.0 ± 7.5 nm) and nearly neutral zeta potential (−0.95 ± 0.65 mV) of GNP-NHN═Dox-mPEG granted the conjugate a long plasma half-life and a slow elimination rate in circulation.

In addition, the chemical structure of the Dox derivative has been designed to achieve not only high stability in circulation, but also selective drug release inside tumor cells via a two-step stimulus-responsive mechanism. The conjugate is taken up by tumor cells mainly via a mechanism of clathrin-mediated endocytosis and then located in lysosomes to liberate Dox-mPEG segments under the acidic environment. After the conjugate escapes from lysosomes, free Dox is released through the esterolysis of the Dox-mPEG in the cytoplasm and enters the nucleus to achieve its effect. The higher antitumor efficacy of GNP-NHN═Dox-mPEG compared to Dox·HCl is shown not only in the suppression of tumor growth, but also in higher intratumoral drug concentrations. Therefore, the results demonstrated in this work confirmed that molecular design is a basic and vital way to modulate *in vitro* and *in vivo* properties and functionalities of nanocarriers and improve their performance and safety in tumor therapeutics.

■ ASSOCIATED CONTENT

Supporting Information

The Supporting Information is available free of charge on the ACS Publications website at DOI: 10.1021/acsami.6b16669.

Synthetic procedures of LA-NHN═Dox-mPEG, DHLA-NHN═Dox-mPEG, and Dox-mPEG; FT-IR, ^{1}H NMR, and ^{13} NMR spectra of all starting materials, starting materials, intermediates, and final products of LA-NHN═Dox-mPEG; stability of GNP-NHN═Dox-mPEG in different media; LSCM images of HepG2 cells after the incubation with Dox·HCl for 4 h (PDF)

■ AUTHOR INFORMATION

Corresponding Authors

*E-mail: zhangcan@cpu.edu.cn. Phone: +86-25-83271171. Fax: +86-25-83271171.

*E-mail: ayanju@163.com. Phone: +86-25-83271326. Fax: +86-25-83271326.

ORCID

Hai Qian: 0000-0002-3827-0992

Ya Ding: 0000-0001-6214-5641

Author Contributions

⊥These authors contributed equally to this work.

Notes

The authors declare no competing financial interest.

■ ACKNOWLEDGMENTS

This research study was financially supported by the Natural Science Foundation of China (31470916, 31500769), the Fundamental Research Funds for the Central Universities (2015PT036, 2016PT014), the Priority Academic Program Development of Jiangsu Higher Education Institutions, and the Open Project Program of MOE Key Laboratory of Drug Quality Control and Pharmacovigilance (DQCP2015MS01).

■ REFERENCES

(1) Ding, Y.; Jiang, Z.-W.; Saha, K.; Kim, C. S.; Kim, S. T.; Landis, R. F.; Rotello, V. M. Gold Nanoparticles for Nucleic Acid Delivery. *Mol. Ther.* **2014**, *22* (6), 1075−1083.

(2) Liang, J.-J.; Zhou, Y.-Y.; Wu, J.; Ding, Y. Gold Nanoparticle-Based Drug Delivery Platform for Antineoplastic Chemotherapy. *Curr. Drug Metab.* **2014**, *15* (6), 620−631.

(3) Ding, Y.; Liang, J.-J.; Geng, D.-D.; Wu, D.; Dong, L.; Shen, W.-B.; Xia, X.-H.; Zhang, C. Development of a Liver-Targeting Gold-PEG-Galactose Nanoparticle Platform and the Structure-Function Study. *Part. Part. Syst. Charact.* **2014**, *31* (3), 347−356.

(4) Bao, Q.-Y.; Geng, D.-D.; Xue, J.-W.; Zhou, G.; Gu, S.-Y.; Ding, Y.; Zhang, C. Glutathione-Mediated Drug Release from Tiopronin-Conjugated Gold Nanoparticles for Acute Liver Injury Therapy. *Int. J. Pharm.* **2013**, *446* (1−2), 112−118.

(5) Tom, R. T.; Suryanarayanan, V.; Reddy, P. G.; Baskaran, S.; Pradeep, T. Ciprofloxacin-Protected Gold Nanoparticles. *Langmuir* **2004**, *20* (5), 1909−1914.

(6) Paciotti, G. F.; Kingston, D. G. I.; Tamarkin, L. Colloidal Gold Nanoparticles: A Novel Nanoparticle Platform for Developing Multifunctional Tumor-Targeted Drug Delivery Vectors. *Drug Dev. Res.* **2006**, *67* (1), 47−54.

(7) Gibson, J. D.; Khanal, B. P.; Zubarev, E. R. Paclitaxel-Functionalized Gold Nanoparticles. *J. Am. Chem. Soc.* **2007**, *129* (37), 11653−11661.

(8) Aryal, S.; Grailer, J. J.; Pilla, S.; Steeber, D. A.; Gong, S.-Q. Doxorubicin Conjugated Gold Nanoparticles as Water-Soluble and pH-Responsive Anticancer Drug Nanocarriers. *J. Mater. Chem.* **2009**, *19* (42), 7879−7884.

(9) Wang, F.; Wang, Y.-C.; Dou, S.; Xiong, M.-H.; Sun, T.-M.; Wang, J. Doxorubicin-Tethered Responsive Gold Nanoparticles Facilitate Intracellular Drug Delivery for Overcoming Multidrug Resistance in Cancer Cells. *ACS Nano* **2011**, *5* (5), 3679−3692.

(10) Manju, S.; Sreenivasan, K. Gold Nanoparticles Generated and Stabilized by Water Soluble Curcumin-Polymer Conjugate: Blood Compatibility Evaluation and Targeted Drug Delivery onto Cancer Cells. *J. Colloid Interface Sci.* **2012**, *368* (1), 144−151.

(11) Joshi, P.; Chakraborty, S.; Dey, S.; Shanker, V.; Ansari, Z. A.; Singh, S. P.; Chakrabarti, P. Binding of Chloroquine-Conjugated Gold Nanoparticles with Bovine Serum Albumin. *J. Colloid Interface Sci.* **2011**, *355* (2), 402−409.

(12) Liong, M.; Lu, J.; Kovochich, M.; Xia, T.; Ruehm, S. G.; Nel, A. E.; Tamanoi, F.; Zink, J. I. Multifunctional Inorganic Nanoparticles for Imaging, Targeting, and Drug Delivery. *ACS Nano* **2008**, *2* (5), 889−896.

(13) Ryu, J. H.; Koo, H.; Sun, I.-C.; Yuk, S. H.; Choi, K.; Kim, K.; Kwon, I. C. Tumor-Targeting Multi-Functional Nanoparticles for Theragnosis: New Paradigm for Cancer Therapy. *Adv. Drug Delivery Rev.* **2012**, *64* (13), 1447−1458.

(14) Dykman, L. A.; Khlebtsov, N. G. Uptake of Engineered Gold Nanoparticles into Mammalian Cells. *Chem. Rev.* **2014**, *114* (2), 1258−1288.

(15) Lee, S.-M.; Kim, H. J.; Kim, S. Y.; Kwon, M.-K.; Kim, S.; Cho, A.; Yun, M.; Shin, J.-S.; Yoo, K.-H. Drug-Loaded Gold Plasmonic Nanoparticles for Treatment of Multidrug Resistance in Cancer. *Biomaterials* **2014**, *35* (7), 2272−2282.

(16) Gu, Y.-J.; Cheng, J.-P; Man, C. W.-Y.; Wong, W.-T.; Cheng, S. H. Gold-Doxorubicin Nanoconjugates for Overcoming Multidrug Resistance. *Nanomedicine* **2012**, *8* (2), 204−211.

(17) Rautio, J.; Kumpulainen, H.; Heimbach, T.; Oliyai, R.; Oh, D.; Järvinen, T.; Savolainen, J. Prodrugs: Design and Clinical Applications. *Nat. Rev. Drug Discovery* **2008**, *7* (3), 255−270.

(18) Ding, Y.; Zhang, P.; Tang, X.-Y.; Zhang, C.; Ding, S.; Ye, H.; Ding, Q.-L.; Shen, W.-B.; Ping, Q.-N. PEG Prodrug of Gambogic Acid: Amino Acid and Dipeptide Spacer Effects. *Polymer* **2012**, *53* (8), 1694−1702.

(19) Paciotti, G. F.; Myer, L.; Weinreich, D.; Goia, D.; Pavel, N.; McLaughlin, R. E.; Tamarkin, L. Colloidal Gold: A Novel Nanoparticle

DOI: 10.1021/acsami.6b16669
ACS Appl. Mater. Interfaces 2017, 9, 8569−8580

Vector for Tumor Directed Drug Delivery. *Drug Delivery* **2004**, *11* (3), 169−183.
(20) Ding, Y.; Zhou, Y.-Y.; Chen, H.; Geng, D.-D.; Wu, D.-Y.; Hong, J.; Shen, W.-B.; Hang, T.-J; Zhang, C. The Performance of Thiol-Terminated PEG-Paclitaxel-Conjugated Gold Nanoparticles. *Biomaterials* **2013**, *34* (38), 10217−10227.
(21) Bao, Q.-Y.; Zhang, N.; Geng, D.-D.; Xue, J.-W.; Merritt, M.; Zhang, C.; Ding, Y. The Enhanced Longevity and Liver Targetability of Paclitaxel by Hybrid Liposomes Encapsulating Paclitaxel-Conjugated Gold Nanoparticles. *Int. J. Pharm.* **2014**, *477* (1−2), 408−415.
(22) Zhang, N.; Chen, H.; Liu, A.-Y.; Shen, J.-J.; Shah, V.; Zhang, C.; Hong, J.; Ding, Y. Gold Conjugate-Based Liposomes with Hybrid Cluster Bomb Structure for Liver Cancer Therapy. *Biomaterials* **2016**, *74*, 280−291.
(23) Lu, X.-L; Howard, M. D.; Talbert, D. R.; Rinehart, J. J.; Potter, P. M.; Jay, M.; Leggas, M. Nanoparticles Containing Anti-Inflammatory Agents as Chemotherapy Sdjuvants II: Role of Plasma Esterases in Drug Release. *AAPS J.* **2009**, *11* (1), 120−122.
(24) Shubayev, V. I.; Pisanic, T. R., II; Jin, S. Magnetic Nanoparticles for Theragnostics. *Adv. Drug Delivery Rev.* **2009**, *61* (6), 467−477.
(25) Stützel, B.; Miyamoto, T.; Cantow, H. J. Hypochromic Effects in UV Spectra of Polymers in Solution. *Polym. J.* **1976**, *8*, 247−253.
(26) Acuna, G. P.; Bucher, M.; Stein, I. H.; Steinhauer, C.; Kuzyk, A.; Holzmeister, P.; Schreiber, R.; Moroz, A.; Stefani, F. D.; Liedl, T.; Simmel, F. C.; Tinnefeld, P. Distance Dependence of Single-Fluorophore Quenching by Gold Nanoparticles Studied on DNA Origami. *ACS Nano* **2012**, *6* (4), 3189−3195.
(27) Chowdhury, S.; Wu, Z.-K; Jaquins-Gerstl, A.; Liu, S.-P; Dembska, A.; Armitage, B. A.; Jin, R.-C; Peteanu, L. A. Wavelength Dependence of the Fluorescence Quenching Efficiency of Nearby Dyes by Gold Nanoclusters and Nanoparticles: The Roles of Spectral Overlap and Particle Size. *J. Phys. Chem. C* **2011**, *115* (4), 20105−20112.
(28) Chen, Y.-F.; Hong, J.; Wu, D.-Y.; Zhou, Y.-Y.; D'Ortenzio, M.; Ding, Y.; Xia, X.-H. *In vivo* Mapping and Assay of Matrix Metalloproteases for Liver Tumor Diagnosis. *RSC Adv.* **2016**, *6* (10), 8336−8354.
(29) Ding, Y.; Xia, X.-H.; Zhang, C. Synthesis of Metallic Nanoparticles Protected with N, N, N-Trimethyl Chitosan Chloride via a Relatively Weak Affinity. *Nanotechnology* **2006**, *17* (16), 4156−4162.
(30) Vaupel, P. Tumor Microenvironmental Physiology and its Implications for Radiation Oncology. *Semin. Radiat. Oncol.* **2004**, *14* (3), 198−206.
(31) Murphy, R. F.; Powers, S.; Cantor, C. R. Endosome pH Measured in Single Cells by Dual Fluorescence Flow Cytometry: Rapid Acidification of Insulin to pH 6. *J. Cell Biol.* **1984**, *98* (5), 1757−1762.
(32) Qiu, N.-S; Liu, X.-R; Zhong, Y.; Zhou, Z.-X; Piao, Y.; Miao, L.; Zhang, Q.-Z; Tang, J.-B; Huang, L.; Shen, Y.-Q. Esterase-Activated Charge-Reversal Polymer for Fibroblast-Exempt Cancer Gene Therapy. *Adv. Mater.* **2016**, *28* (48), 10613−10622.
(33) Saha, K.; Kim, S. T.; Yan, B.; Miranda, O. R.; Alfonso, F. S.; Shlosman, D.; Rotello, V. M. Surface Functionality of Nanoparticles Determines Cellular Uptake Mechanisms in Mammalian Cells. *Small* **2013**, *9* (2), 300−305.
(34) Shukla, R.; Bansal, V.; Chaudhary, M.; Basu, A.; Bhonde, R. R.; Sastry, M. Biocompatibility of Gold Nanoparticles and Their Endocytotic Fate Inside the Cellular Compartment: A Microscopic Overview. *Langmuir* **2005**, *21* (23), 10644−10654.
(35) Patolsky, F.; Katz, E.; Willner, I. Amplified DNA Detection by Electrogenerated Biochemiluminescence and by the Catalyzed Precipitation of an Insoluble Product on Electrodes in the Presence of the Doxorubicin Intercalator. *Angew. Chem., Int. Ed.* **2002**, *41* (18), 3398−3402.
(36) Lodish, H.; Berk, A.; Matsudaira, P.; Kaiser, C. A.; Krieger, M.; Scott, M. P.; Zipursky, S. L.; Darnell, J. *Molecular Cell Biology*, 5th ed.; WH Freeman: New York, 2004.
(37) Tacar, O.; Sriamornsak, P.; Dass, C. R. Doxorubicin: An Update on Anticancer Molecular Action, Toxicity and Novel Drug Delivery Systems. *J. Pharm. Pharmacol.* **2013**, *65* (2), 157−170.
(38) Carvalho, F. S.; Burgeiro, A.; Garcia, R.; Moreno, A. J.; Carvalho, R. A.; Oliveira, P. J. Doxorubicin-Induced Cardiotoxicity: From Bioenergetic Failure and Cell Death to Cardiomyopathy. *Med. Res. Rev.* **2014**, *34* (1), 106−135.
(39) Maeda, H.; Wu, J.; Sawa, T.; Matsumura, Y.; Hori, K. Tumor Vascular Permeability and the EPR Effect in Macromolecular Therapeutics: A Review. *J. Controlled Release* **2000**, *65* (1−2), 271−284.

DOI: 10.1021/acsami.6b16669
ACS Appl. Mater. Interfaces 2017, 9, 8569−8580